Arabian Journal for Science and Engineering (2024) 49:15597–15610
https://doi.org/10.1007/s13369-024-09134-y

RESEARCH ARTICLE-MECHANICAL ENGINEERING

The Fan Design Optimization for Totally Enclosed Type Induction Motor with Experimentally Verified CFD-Based MOGA Simulations

Tufan Özyildiz[1] · **Senem Şentürk Lüle**[1]

Received: 21 December 2023 / Accepted: 25 April 2024 / Published online: 22 May 2024

Abstract
The energy efficient electric motors save energy thus reduce operating costs. Since there are several losses affecting the motor efficiency, fan design plays an important role to minimize these losses. This study examines the effects of the design parameters of a radial bladed fan on the motor efficiency in a 132 frame with a power of 7.5 kW. The parametric analysis was carried out with the computational fluid dynamics method, and the results were used for the multiobjective genetic algorithm (MOGA) optimization study with the highest efficiency and the lowest motor body temperature objectives. The hub height, hub radius, distance to body cover, blade rising angle, fan cover entrance distance, blade edge angle, blade center radius, blade edge radius, blade end radius, and center edge distance were selected as optimization parameters. 151 simulations were performed. The results showed that the most important parameter for fan efficiency is the hub height which is the parameter that determines the height of the fan impeller diameter. According to the results, the optimum fan design increased the efficiency by 8% compared to the original fan and reduced the winding temperature by 8 °C. The optimized fan design was manufactured and tested against imulation data. This study contributes to sustainable development goals by improving motor efficiency that reduces the cost, designing of new components, and cooling the fan effectively that reduces the amount of copper used.

Keywords Enclosed induction motor · Fan design optimization · Efficiency · Computational fluid dynamics · MOGA

Abbreviations

CFD	Computational fluid dynamics
CV	Control volume
DOE	Design of experiments
GA	Genetic algorithm
MOGA	Multiobjective generic algorithm
RSM	Reynolds stress model
SST	Shear stress transport

List of Symbols

D	Diameter of the impeller
D_ω	Cross-diffusion term
E	Energy
$\vec{F}$	Body force
$\vec{g}$	Gravitational acceleration
G_k	Production of turbulence kinetic energy
G_ω	Generation of specific dissipation rate
h_j	Specific enthalpy of species j
J_j	Mass flux of species j
k	Turbulence kinetic energy
N	Rotational speed
P	Pressure difference
p	Static pressure
$P_{hydraulic}$	Hydraulic power
P_{shaft}	Shaft power
Q	Volumetric flow rate
Re	Reynolds number
S_h	Volumetric heat source
$\vec{v}$	Velocity vector

Greek Symbols

ρ	Density

✉ Senem Şentürk Lüle
senturklule@itu.edu.tr

[1] İstanbul Technical University, Energy Institute, Istanbul, Turkey

η	Fan efficiency
Γ	Effective diffusivity
μ	Viscosity
ω	Angular velocity, Specific dissipation rate
$\overline{\overline{\tau}}$	Stress tensor
τ	Torque

1 Introduction

The motor-driven systems consume 40% of global electricity per year, and 70% of this consumption is used by the industry [1]. Thus, to reduce carbon footprint and help sustainable development goals, European Commission published a new regulation about the efficiency limits in 2019 [2]. The idea was to save 10 TWh energy until 2030 with the increase in efficiency level of electric motors. There are 17 sustainable development goals which are an urgent call for action by all countries—developed and developing—in a global partnership [3]. Especially the goals 7, 9, 11, and 12 which are affordable and clean energy, industry, innovation and infrastructure, sustainable cities and communities, and responsible consumption and production, respectively, can be correlated with the increase of efficiency of electricity motors. Special types of motors differ according to the purpose of use and include synchronous reluctance [4], stepper motor [5], brushless motor [6], hysteresis [7], and universal [8] types. Today, asynchronous [9] motors are widely used due to their low production cost, simple structure, and reliability in harsh operating conditions. Totally enclosed type induction motors can be used for heating, ventilation, air conditioning, cooling, and smoke extraction. During operation, they face challenges either due to excess production of heat or due to insufficient airflow because of being in an enclosed space.

In the literature, analytical methods or numerical methods are implemented for thermal analysis of induction motors. The analytical method is simple and rapid but limited in terms of a temperature distribution while computational fluid dynamics (CFD) is more accurate especially for complex geometries but rather time consuming [10]. Several properties affecting the efficiency of electric motors such as the number of fins on the electric motor, the fan blade form, and the air gap between the stator and rotor have been studied. The axial fan performance and noise for heavy electric vehicles were investigated, and the results were compared with two commercial fans of SCANIA [11]. The Taylor Coutte dimensionless numbers were investigated in order to understand heat transfer rate in high round per minute (rpm) traction motor by applying, $k-\omega$ shear stress transport (SST) turbulence method for boundary layer solutions and by using $y+$ between 0 and 100 [12]. The axial and radial fans were examined both experimentally and numerically to show that one of the axial fan designs improved motor efficiency while keeping the temperature constant [13]. The performance studies conducted on two separate fans to examine the cooling performance with Autodesk CFD 2013 software showed that the cooling with the axial fan was slightly lower than the radial fan [14]. The study on air gap between the stator and rotor in rotating electrical machines successfully verified the simulation outputs of six correlation equations given in the literature [15]. A motor cooling system examination with a focus on fins showed that increasing the number of fins did not adversely affect the cooling performance because it increased the surface area, although it decreased the flow [16]. An investigation on the heat transfer parameters of induction motor and the importance of the convection coefficient and mass flow rate concluded that increasing of mass flow rate twice reduces the winding temperatures around 10 °C [17]. The optimization study about the fins on the 400-frame motor was done with 2600 2D simulations. It was determined that the 9-fin variant was the best for 400 frames and it was stated that the maximum temperature difference in all results was 19 °C and increasing the blade thickness after a certain value was not beneficial as it blocked the flow [18]. The parametric analysis of impeller shape and the number of blades was performed to determine the mathematical relationship useful for the sizing of a fan. The results showed that for a given blade number, the dimensionless flow capacity depends on the aspect ratio of the impeller and for a given geometry, there is an optimal number of blades that maximizes the flow rate processed by the fan [19].

This study aims to contribute global sustainable development goals while investigating the effects of design parameters of a 3-phase totally enclosed fan for 7.5 kW asynchronous induction motor to provide cost and efficiency advantage by increasing the cooling performance on the body. The study includes parametric design of fan, preparing the geometry for simulation, deciding solution methodology, experimentation, and optimization studies performed with CFD code ANSYS Fluent [20]. The optimization problems usually are carried out with analytical models to speed out the decision making despite there is a loss of accuracy [21, 22]. On the other hand, this study uses more accurate CFD methodology. ANSYS Design Modeler was used for the parametric design, ANSYS Mesh for the mesh generation, ANSYS FLUENT for solver, and ANSYS Design Exploration for optimization study. The design optimization of the radial fan geometry was aimed with multiobjective genetic algorithm (MOGA).

2 Mathematical Modeling

There are several losses that affect the efficiency of an electric motor such as joule loss, eddy current loss, hysteresis loss, bearing loss, and windage loss which are correlated with current, resistance rotational speed of shaft, diameter of rotor, rotor length, average magnetic field density, and fluid density [23]. The cooling improvement work for the fan component in the motor has a positive effect on the efficiency and operating performance. Along with fan theory [24], conductive, convective, and radiative heat transfer [25] must be considered for cooling calculations.

Within the electric motor, there is a conduction between the stator and the body due to their press fit connection and between the stator grooves and the insulation materials and the copper windings. In totally enclosed type electric motor, the fan working with motor rounds per minute (rpm) provides flow between the fins by the direction of the fan cover and therefore sustains major convective heat transfer. For this reason, besides the well-designed fan, the geometric details of the fin structure in the motor are important in terms of the cooling performance. The radiation heat transfer was neglected in this study since temperature difference is not very high.

The problem covered in this study was simulated by using steady state; therefore, conservation equations were given in steady state. The conservation of mass can be used to calculate displacements in a given control volume (Eq. 1 [26]).

$$\nabla \cdot (\rho \vec{v}) = 0 \tag{1}$$

where ρ is the density and $\vec{v}$ is the velocity vector.

The conservation of momentum (Eq. 2 [26]) states that particle system in a control volume is the sum of the external force acting on it.

$$\nabla \cdot (\rho \vec{v}\vec{v}) = -\nabla p + \nabla \cdot \left(\overline{\overline{\tau}}\right) + \rho \vec{g} + \vec{F} \tag{2}$$

where p is the static pressure, $\overline{\overline{\tau}}$ is the stress tensor, and $\rho \vec{g}$ and $\vec{F}$ are the gravitational body force and external body forces.

The energy equation mathematically explains the addition or subtraction of the energy of the control volume (Eq. 3 [26]).

$$\nabla \cdot (\vec{v}(\rho E + p)) = -\nabla \cdot \left(\sum_j h_j J_j \right) + S_h \tag{3}$$

where E is the energy, h_j is specific enthalpy of species j, J_j is the mass flux of species j, and S_h is the volumetric heat source.

The correlation of target data such as volume flow rate and power with the change of the geometric properties of the fan has been examined and led to the fan laws, which are widely used in the industry, since they provide average results. The first of correlation is volume flow capacity (Eq. 4 [27]).

$$\frac{Q_1}{Q_2} = \left(\frac{N_1}{N_2}\right)\left(\frac{D_1}{D_2}\right)^3 \tag{4}$$

where Q is the volumetric flow rate, N is the rotational speed of the impeller, and D is the diameter of the impeller.

The second of the correlations is head or pressure (Eq. 5 [27]).

$$\frac{dP_1}{dP_2} = \left(\frac{N_1}{N_2}\right)^2\left(\frac{D_1}{D_2}\right)^2 \tag{5}$$

where P is the pressure difference created by the fan. Equation 5 is used frequently to create quick predictions, especially in the studies carried out to find the best efficient point in fan design.

The third correlation (Eq. 6 [27]) implies that the power that the fan expends by being driven is proportional to cube of the rate of rotation and fifth power of the impeller diameter.

$$\frac{P_1}{P_2} = \left(\frac{N_1}{N_2}\right)^3\left(\frac{D_1}{D_2}\right)^5 \tag{6}$$

Although the fan theory equations are sufficient to get fast results in air conditioning studies, these equations lose their validity for electric motors where the effect of the velocity profile on a body cover is examined. In order to examine the cooling effect of the velocity profile on the body, the effect of all design parameters besides the impeller diameter should be investigated. It will be a very long and costly process to produce and test different geometries one by one for the geometry improvement. For this reason, computational methods are of a critical importance in research and development activities.

Since ANSYS Fluent CFD code uses a control volume-based (CV) technique, it converts a general transport equation into an algebraic equation which is numerically solvable. The CV technique integrates the transport equation about each control volume and therefore yields a discrete equation that expresses the conservation law on a control volume basis.

3 Preparation of CFD Model

Computational fluid dynamics studies, especially optimization studies, have become indispensable for research and

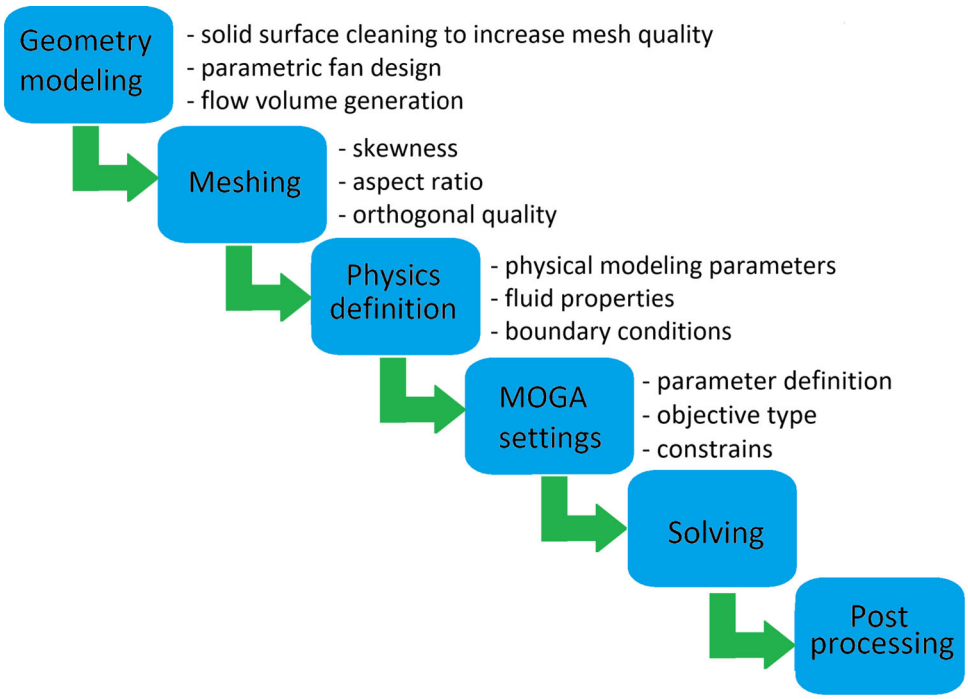

Fig. 1 The methodology of the study

development to save time and money. However, certain procedures must be done before the optimization study. The methodology followed in this study is summarized in Fig. 1.

First of all, the output requirements must be determined and the geometry and the mesh must be robust. Since many parameter combinations will be tried automatically during the optimization, it is necessary to ensure that unexpected volumes will not occur due to change in parameters. In addition, the properties of the mesh such as mesh quality and y^+ values should be the same for all parameter solutions. Furthermore, sufficient trials should be performed within the optimization study.

Before moving on to the calculation methodology, solid surface cleaning work that is removing the details on the body that will not affect the phenomenon and removing the edges and surfaces that will cause a decrease in mesh quality values were performed. The radiuses on the geometry, especially on the fin edges and facilitating the mold output, bolt details in the terminal box, and foot windows and details with the prediction of no interference with the flow profile driven from fan were removed to prevent possible problems during meshing and the surfaces were repaired. The original (unclean) and clean motor geometries are shown in Fig. 2.

After the solid model surface cleaning process, the parametric fan design and the flow volume were created. For the parametric fan design, since the motor is a totally enclosed type induction motor, the parameter limits of the fan design are on the fan cover and the body. This information is critical in terms of determining the lower and upper limits to which the design parameters will be tested. The parametric design started with fan hub by determining five parameters; the impeller length of the fan, the axial length of the upper and lower points of the fan to the cover, and the radius and thickness of the geometry drawn as arc. Afterwards, blade designs were formed by determining four parameters: angle between the shaft connecting edge and the upper blade edge, the distance of the upper edge of the fan blade to the fan cover, the blade elevation angle of the edge between the fan shaft edge, and the top edge, and the length of the shaft edge.

After the blade geometric form was connected to the parameter, blend parameters were also included in order to optimize the velocity profile for target outputs.

The number of blades was not included in the parameter list for optimization since inclusion, most definitely, will increase the computational load. However, the number was set to 7 before optimization study according to requirements of the manufacturer that this study was performed. Parametrically completed fan geometry is shown in Fig. 3. As the last step before the optimization study, the fluid flow volume was created and the product tree in the design models was followed automatically in the parameter changes made afterward.

Before starting the optimization analysis, the position of the target outputs should be determined and names should be given to these surfaces or volumes. Since flow rate and fan design parameters are the outputs for evaluation, the volume inside the fan cover was treated separately. After the fan cover flow volume was separated, the resulting flow volume for simulation work is shown in Fig. 4. However, it should be noted that a share topology must be made between the

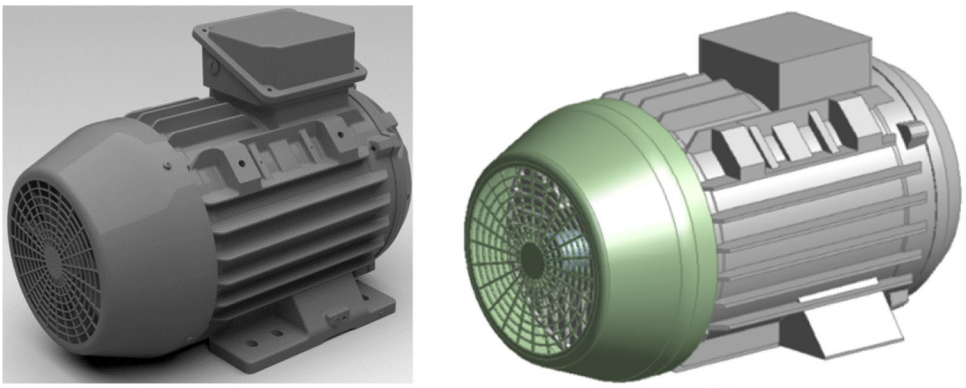

(a) (b)

Fig. 2 The geometry of motor **a** original (unclean), **b** clean

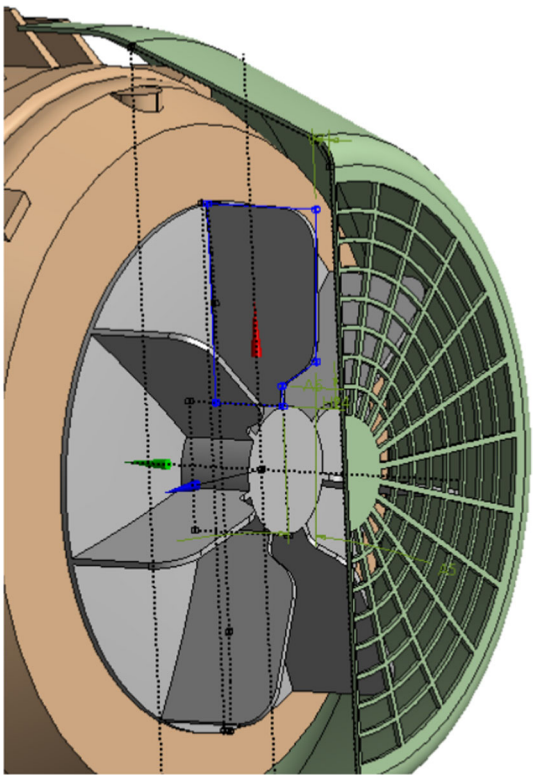

Fig. 3 The parametric fan generated for optimization study

flow volumes. Otherwise, incorrect results will be obtained because the mesh connection between the geometries cannot be provided in the mesh work.

The determination of the boundary conditions on the motor and selection of the discretization methods and turbulence method were performed. According to the data obtained from the experiments, the total heat flux is 8192 W/m^2 in the steady condition between the stator and the body. While the rotational speed of the motor is 1500 rpm, it is expected that the amount of loss experienced by the motor during rotation is the sum of the fan and bearing loss. The ambient operating temperature of the motor was taken as 27 °C as in experimental studies.

Table 1 Mesh independency test results

	$k-\omega$ simulation flow rate results (L/s)
8	54.9
12	56.4
18	55.5

The preparation of geometry and mesh studies are iterative processes within themselves due to mesh quality issue. The mesh quality values followed in this study are skewness, aspect ratio, and orthogonal quality. In parametric analysis, the quality values should not reach to a critical point with the change of the parameters; therefore, maximum quality value of 0.85 for maximum skewness, 30 for maximum aspect ratio, and 0.7 for minimum orthogonal quality were selected.

Three different meshes with 8 million, 12 million, and 18 million elements were studied in order to prove mesh independency. By considering the flow rate results of the mesh independency study given in Table 1, 12 million mesh was selected to reduce the computational load. The final computational mesh is shown in Fig. 5.

In order to filter and compare the fluid properties that change with the change of fan parameters, measurements must be taken from predetermined locations on the geometry. These locations are shown in Fig. 6. In order to calculate the fan power, the torque value on the blades, the pressure and flow values on the fan cover inlet grille and outlet grille, and the temperature values on the body were taken.

Although plots included in the evaluation give the defined outputs at a certain location, it is necessary to write the fan efficiency equation for optimization study. The fan efficiency (η) can be written as the ratio of hydraulic power ($P_{\text{hydraulic}}$) and the shaft power (P_{shaft}) as seen in Eq. (7) [28].

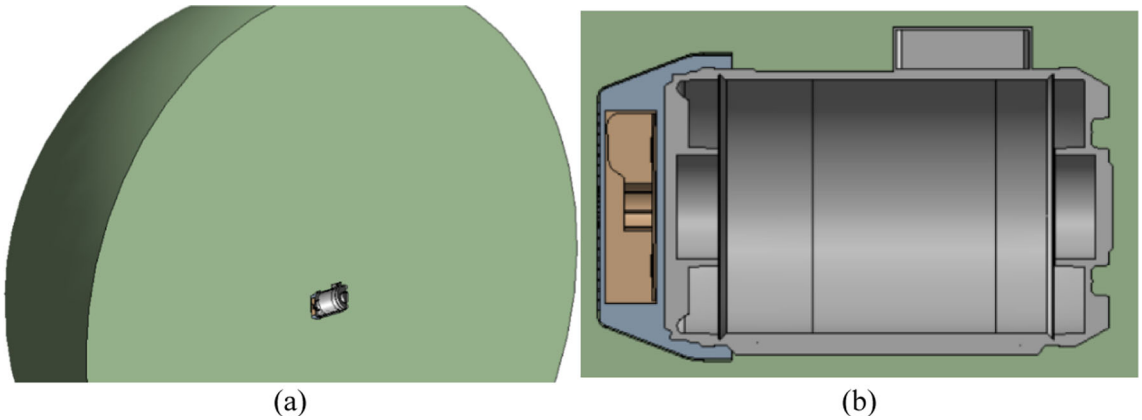

Fig. 4 The geometry view **a** enclosure, **b** section

Fig. 5 The mesh enclosure view **a** and section view **b**

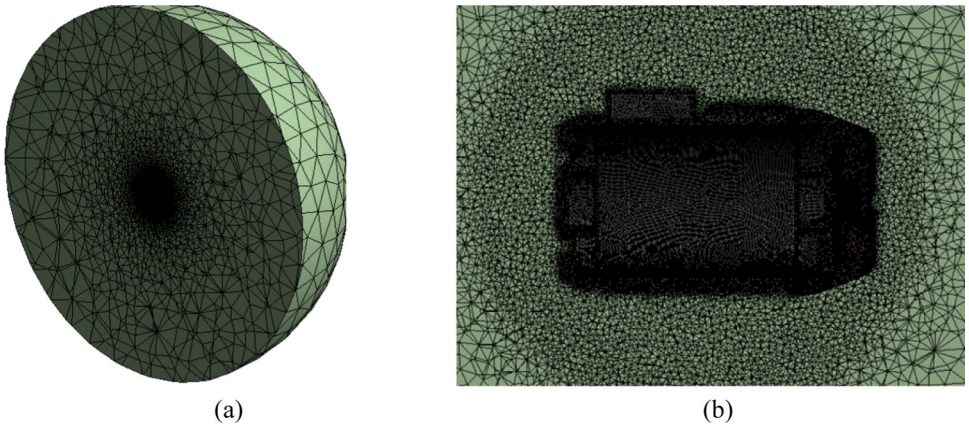

Fig. 6 Result collection locations **a** total view, **b** cut view

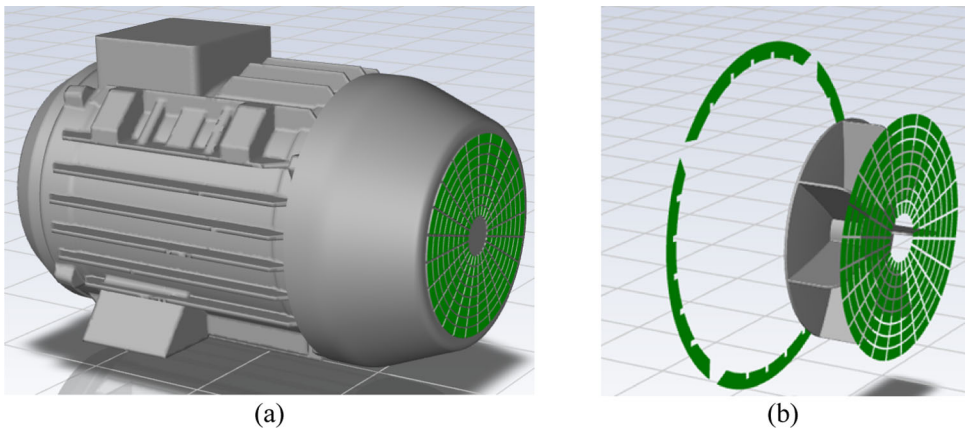

$$\eta = \frac{P_{\text{hydraulic}}}{P_{\text{shaft}}} \tag{7}$$

The hydraulic power is the multiplication of the volume flow rate (Q) and the total pressure difference (P) at the fan cover inlet and outlet (Eq. 8). The shaft power can be written as the multiplication of the torque (τ) and angular velocity (ω) as seen in Eq. (9).

$$P_{\text{hydraulic}} = \text{Q} \times (P_{\text{total, in}} - P_{\text{total, out}}) \tag{8}$$

$$P_{\text{shaft}} = \tau \times \omega \tag{9}$$

Fig. 7 Test environment of the motor with commercial fan

Table 2 Characteristics values of the motor with commercial fan

Parameter	Value
Experiment end winding temperature (°C)	88.0 ± 0.2
Motor efficiency (%)	89.21
Fan volumetric flow rate (L/s)	57.2 ± 0.5
Fan efficiency (%)	40
Simulation average temperature distribution on body (°C)	50.1

Table 3 Validation of turbulence model with anemometer experiment

Model	Simulation flow rate result (L/s)	Experiment flow rate result (L/s)	Relative error (%)
$k-\omega$	56.4	57.2 ± 0.5	1.39
$k-\varepsilon$	61.0	57.2 ± 0.5	6.64
RSM	59.0	57.2 ± 0.5	3.14

In addition to the parameters such as fan efficiency and fan power, the temperature values from the body and the efficiency test on the dynamometer were also used to optimize the fan design.

3.1 Validation of the CFD Model

In order to validate the CFD model, two experiments of 30 min were performed. The first 20 min of the experiments were for making the motor to reach operating regime. The data were acquired in the last 10 min of the experiments. The average of two tests were used for validation study. A test environment is shown in Fig. 7. The flow rate data and temperature data from the simulations were compared with 3 anemometer flow rate tests and 3 thermocouple tests, respectively. The test results are given in Table 2.

Firstly, $k-\omega$ SST, $k-\varepsilon$ realizable, and RSM enhanced wall treatment turbulence method simulation results were compared with each other and with the experimental data. Table 3 shows that flow rate results are in good agreement with the experimental results. However, $k-\omega$ SST model makes better prediction; therefore, the simulations were completed with $k-\omega$ SST model.

The $k-\omega$ model is an empirical model based on model transport equations for the turbulence kinetic energy (k) and the specific dissipation rate (ω). In the $k-\omega$ SST model, there is a gradual change from the standard $k-\omega$ model in the inner region of the boundary layer to a high Reynolds number version of the $k-\varepsilon$—model in the outer part of the boundary layer and there is a modified turbulent viscosity formulation to account for the transport effects of the principal turbulent shear stress. The $k-\omega$ model transport equations are given in Eqs. (10) and (11) [26].

$$\frac{\partial}{\partial t}(\rho k)+\frac{\partial}{\partial x_i}(\rho k u_i)=\frac{\partial}{\partial x_i}\left[\Gamma_k\frac{\partial k}{\partial x_i}\right]+G_k-Y_k+S_k+G_b \tag{10}$$

$$\frac{\partial}{\partial t}(\rho\omega)+\frac{\partial}{\partial x_i}(\rho\omega u_i)=\frac{\partial}{\partial x_j}\left[\Gamma_\omega\frac{\partial \omega}{\partial x_j}\right]+G_\omega - Y_\omega+D_\omega+S_\omega+G_{\omega b} \tag{11}$$

where G_k represents the production of turbulence kinetic energy, G_ω represents the generation of ω, Γ_k and Γ_ω represent the effective diffusivity of k and ω, Y_k and Y_ω represent the dissipation of k and ω due to turbulence, D_ω represents the cross-diffusion term, S_k and S_ω are user-defined source terms, and $G_{\omega b}$ accounts for buoyancy terms.

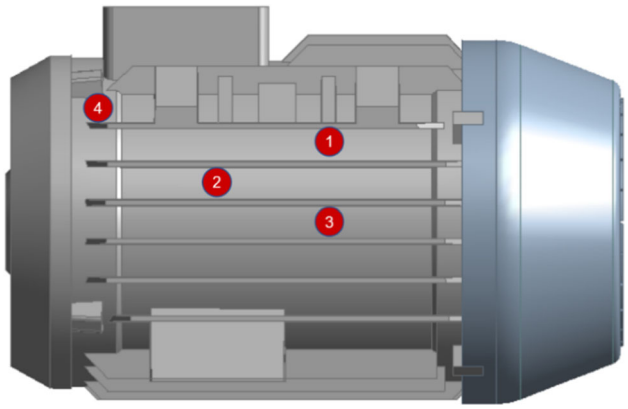

Fig. 8 The thermocouple locations used during experiments

Table 4 Validation of the models and geometry with thermocouple experiment

Points	Simulation temperature result (°C)	Experimental temperature result (°C)	Relative error (%)
1	44	47.3 ± 0.2	6.97
2	52.2	55.7 ± 0.2	6.28
3	41	39.9 ± 0.2	2.8
4	–	88.0 ± 0.2	–

The turbulent viscosity is calculated by using Eq. (12) [26].

$$\mu_t = \frac{\rho k}{\omega} \frac{1}{\max\left[\frac{1}{\alpha^*}, \frac{SF_2}{a_1 \omega}\right]} \tag{12}$$

where S is the strain rate magnitude and α^* is defined in Eq. (13) and F_2 is given by Eq. (14) [26].

$$\alpha^* = \alpha^*_\infty \left(\frac{\alpha^*_0 + Re_t/R_k}{1 + Re_t/R_k}\right) \tag{13}$$

where $\mathrm{Re}_t = \frac{\rho k}{\mu \omega}$ $R_k = 6\,\alpha^*_0 = \frac{\beta_i}{3}$ $\beta_i = 0.072$

$$F_2 = \tanh\left(\emptyset_2^2\right) \tag{14}$$

where $\emptyset_2 = \max\left[2\frac{\sqrt{k}}{0.09\omega y}, \frac{500\mu}{\rho y^2 \omega}\right]$ and y is the distance to the next surface.

The temperature measurements were taken from the four locations marked as 1, 2, 3 (on the body), and 4 (on the winding inside the body) as shown in Fig. 8 when the motor entered the working regime.

The results of thermocouple experiment shown in Table 4 indicate that simulation results agree well with the experimental data. Therefore, the prepared CFD model can be used for the optimization study.

Table 5 Boundaries of design parameters

Parameter	Value
Hub height (mm)	55–78
Hub radius (mm)	200–791
Distance to body cover (mm)	5–15
Blade rising angle (°)	20–70
Fan cover entrance distance (mm)	5–8.5
Blade edge angle (°)	1–7.5
Blade center radius (mm)	3–10
Blade edge radius (mm)	3–15
Blade end radius (mm)	3–15
Center edge distance (mm)	3–15

4 Fan Design Optimization Results

The design of experiment (DOE) studies basically determines the weight coefficient on the parameters based on the results of the combinations of the determined input parameters. This weight is determined from a generic algorithm of ANSYS MOGA. Genetic algorithm (GA) is a population-based algorithm which imitates the natural reproduction system based on Darvin's principle of survival of the fittest [29]. It starts from the generation of the initial population of alternatives called chromosomes. The randomly selected chromosomes from the population are then subjected to mutation, i.e., fitness function evaluation, crossover, i.e., cross-replacements, and selection repeatedly until termination criteria are reached. It works on the local search of the best solution considering fitness evaluation. There are many different applications of GA in engineering problems [30–32].

A set of coefficients was assigned to the target output over the factors determined. Each of the parameters to be evaluated during the parametric drawing should be given a limit range in which the optimization work will be done. However, it should be noted that the given limit range should not be caught by real geometric obstacles. In such a case, incorrect geometries will occur. All of the determined parameters and ranges used in this study are given in Table 5. A total of 151 combinations were extracted with the central composite design method. The MOGA simulations were arranged to have 10,000 samples initially, 2200 samples per iteration, and to find 3 candidates in a maximum of 20 iterations. The simulation was converged after 35,921 evaluations as shown in Fig. 9

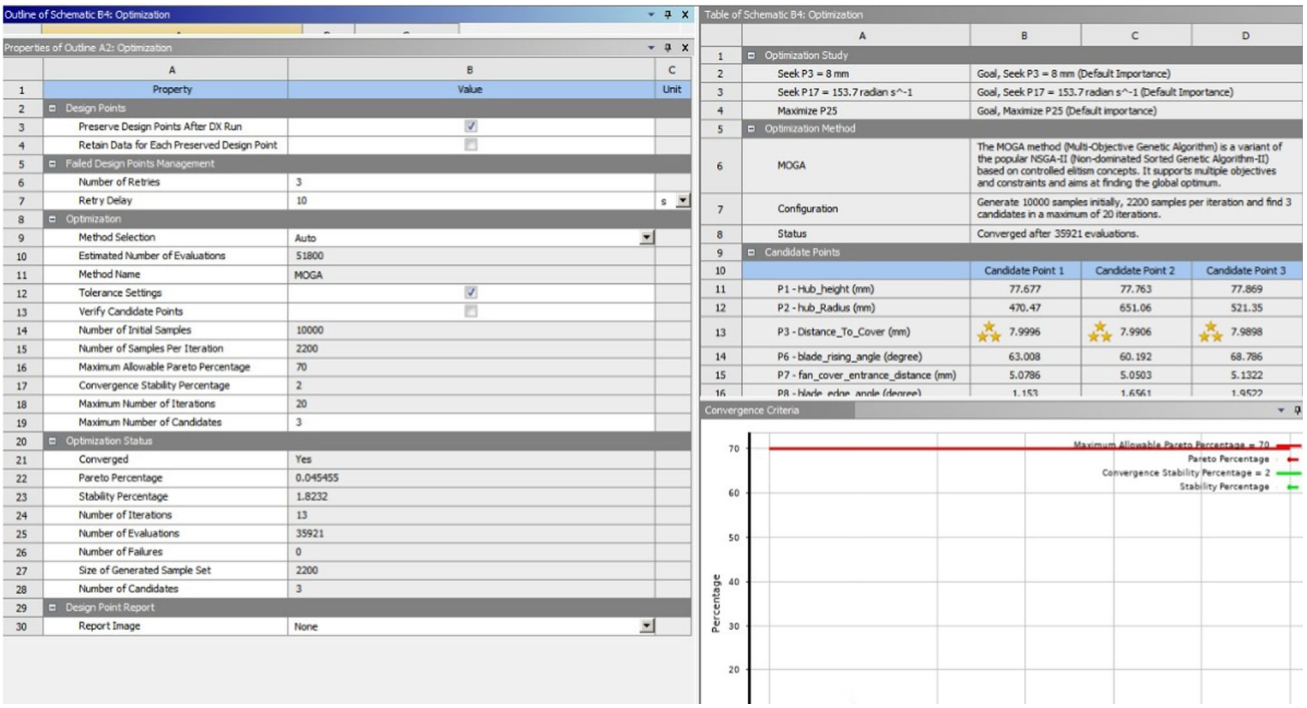

	A	B	C
1	Property	Value	Unit
2	Design Points		
3	Preserve Design Points After DX Run	☑	
4	Retain Data for Each Preserved Design Point	☐	
5	Failed Design Points Management		
6	Number of Retries	3	
7	Retry Delay	10	s
8	Optimization		
9	Method Selection	Auto	
10	Estimated Number of Evaluations	51800	
11	Method Name	MOGA	
12	Tolerance Settings	☑	
13	Verify Candidate Points	☐	
14	Number of Initial Samples	10000	
15	Number of Samples Per Iteration	2200	
16	Maximum Allowable Pareto Percentage	70	
17	Convergence Stability Percentage	2	
18	Maximum Number of Iterations	20	
19	Maximum Number of Candidates	3	
20	Optimization Status		
21	Converged	Yes	
22	Pareto Percentage	0.045455	
23	Stability Percentage	1.8232	
24	Number of Iterations	13	
25	Number of Evaluations	35921	
26	Number of Failures	0	
27	Size of Generated Sample Set	2200	
28	Number of Candidates	3	
29	Design Point Report		
30	Report Image	None	

	A	B	C	D
1	Optimization Study			
2	Seek P3 = 8 mm	Goal, Seek P3 = 8 mm (Default Importance)		
3	Seek P17 = 153.7 radian s^-1	Goal, Seek P17 = 153.7 radian s^-1 (Default Importance)		
4	Maximize P25	Goal, Maximize P25 (Default importance)		
5	Optimization Method			
6	MOGA	The MOGA method (Multi-Objective Genetic Algorithm) is a variant of the popular NSGA-II (Non-dominated Sorted Genetic Algorithm-II) based on controlled elitism concepts. It supports multiple objectives and constraints and aims at finding the global optimum.		
7	Configuration	Generate 10000 samples initially, 2200 samples per iteration and find 3 candidates in a maximum of 20 iterations.		
8	Status	Converged after 35921 evaluations.		
9	Candidate Points			
10		Candidate Point 1	Candidate Point 2	Candidate Point 3
11	P1 - Hub_height (mm)	77.677	77.763	77.869
12	P2 - hub_Radius (mm)	470.47	651.06	521.35
13	P3 - Distance_To_Cover (mm)	7.9996	7.9906	7.9898
14	P6 - blade_rising_angle (degree)	63.008	60.192	68.786
15	P7 - fan_cover_entrance_distance (mm)	5.0786	5.0503	5.1322
16	P8 - blade_edge_angle (degree)	1.153	1.6561	1.9522

Fig. 9 MOGA simulation settings

Figure 10 shows the effect of each individual parameter given in Table 5 on the fan efficiency.

Since the hub height is the parameter that determines the height of the fan design impeller diameter and indirectly determines the blade length and the hub radius is the parameter that determines the radius of this disk, their increase in value increases the fan efficiency as shown in Fig. 10. However, the hub radius seems to have reached the optimum point before reaching its maximum limit.

Figure 10 shows that the effect of the distance from fan-to-fan cover and fan to body cover on fan efficiency is negative with similar slopes. Since it is a bidirectional blade, the blade rising angle is one of the main factors forming the velocity profile. This is highly important in efficiency calculations where there is a thermal response. In addition to geometric properties of the fan, rotational velocity decides the scale of profile. However, it should not be forgotten that the reactions created also depend on the fan cover form. Increasing the blade surface area has a positive effect on fan efficiency.

Although blade surface area has positive effect on fan efficiency, the blade edge angle shows opposite effect (Fig. 10). Since the edge radius removes the inefficient surface area of the radius at the blade, it causes decreasing of the torque and therefore increases the efficiency of fan. The center edge distance defines the point where the blade rising angle starts. Therefore, it is trivial that the greater the distance, the smaller the blade surface area. At the beginning, the distance to the blade lift angle affects the efficiency positively but it has a negative effect on the efficiency toward the upper limit distance. As a result, it can be said that the surface area at the lower limit distance does not have the same effect on the flow increase while increasing the torque.

The error analysis of plotted parameters is given in Table 7, and it shows that the results have high accuracy. The sensitivity pie chart in Fig. 11 shows the effect of parameters considered for optimization in Table 5 on output parameters defined in Table 6. Figure 11 indicates that the most important parameter effecting the efficiency is the hub height.

The MOGA analysis with the highest efficiency and the lowest body average temperature objectives resulted in the optimum fan design with values given in Table 7.

The visual comparison of the optimized fan and the commercial fan is shown in Fig. 12. When visually compared, especially the blade rising angle, end blade radius, and center edge distance are among the factors that make an impact on the results.

The temperature distribution of the motor with commercial fan and optimized fan in Fig. 13 indicates the effective cooling of the motor with the optimized fan.

The increase in efficiency and decrease in end winding temperature shown in Table 8 present the success of the optimization study. The results showed that arc line parameter of the hub and the blend parameters increased the fan efficiency significantly.

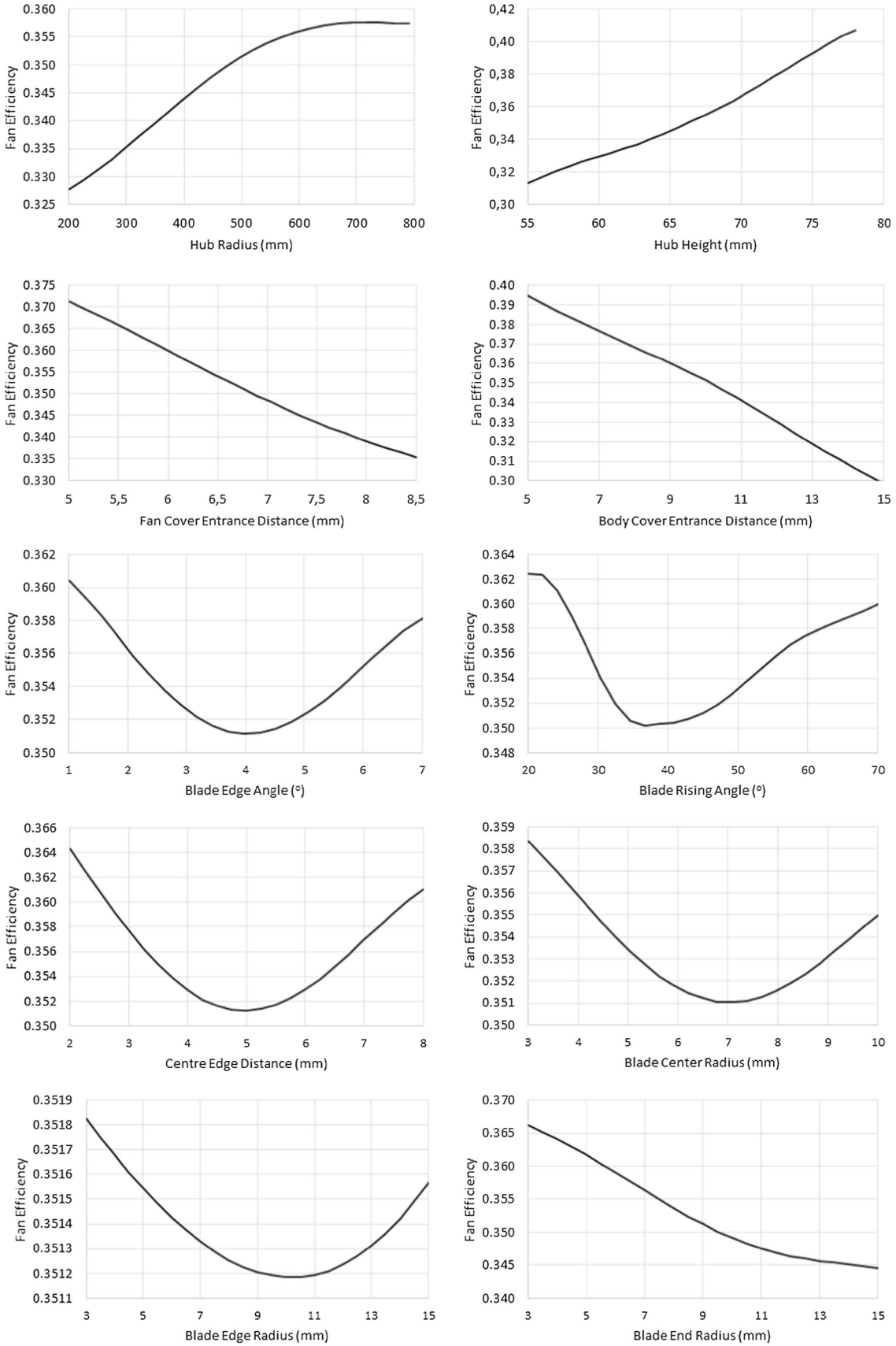

Fig. 10 The effect of design parameters on fan efficiency

Fig. 11 The sensitivity chart

Table 6 Plotted output values from simulations

Variable	Calculated minimum	Calculated maximum	Maximum prediction error	Relative error (%)
Total inlet pressure (Pa)	5.94	131.36	15.46	0.112
Total outlet pressure (Pa)	49.17	471.65	9.94	0.019
Fluid power (W)	9.09	38.98	2.46	0.051
Real power (W)	18.07	101.05	26.05	0.218
Fan efficiency (%)	20.74	49.99	0.006	0.022
Body back cover average temperature (°C)	319.8	351.6	3.86	0.121
Body front cover average temperature (°C)	303.4	313.1	1.11	0.115
Blade torque (Nm)	0.02	0.34	0.024	0.065
Volumetric flow rate (m^3/s)	0.025	0.129	0.006	0.061

Table 7 Optimum design values of parameters from MOGA analysis

Parameter	Value
Hub height (mm)	75.64
Hub radius (mm)	713.24
Distance to body cover (mm)	7.99
Blade rising angle (°)	62.99
Fan cover entrance distance (mm)	5.00
Blade edge angle (°)	1.55
Blade center radius (mm)	4.786
Blade edge radius (mm)	7.58
Blade end radius (mm)	3.27
Center edge distance (mm)	2.39

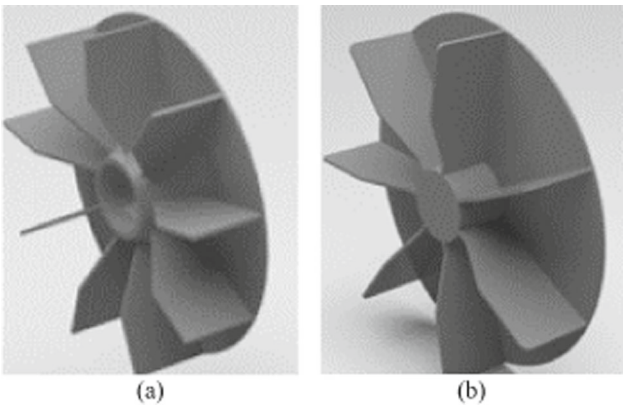

Fig. 12 The commercial fan **a** and the optimized fan **b**

5 Conclusions

The fan optimization was studied for the totally enclosed type induction motor with multiobjective genetic algorithm (MOGA). The inclusion of both the fan cover which brings limitations on the fan and the impact of the fin geometry which increases the flow friction coefficient in the parametric studies added a value to this study.

The results showed that the parameter which contributes the most to the motor efficiency and flow rate is hub height which is the parameter that determines the height of the fan design impeller diameter. Although impeller diameter increases the fan power, blade lift angle, impeller arc, and blade lift blends have relatively less contribution to fan power consumption. On the other hand, their contribution to efficiency is high. At the end of the optimization study, the optimized fan was produced and tested and passed the evaluation tests successfully.

Table 8 Comparison of commercial and optimized fan

	Commercial	Optimized
Experiment end winding temperature (°C)	88	80
Motor efficiency (%)	89.21	89.21
Fan volumetric flow rate (L/s)	57.2	68
Fan efficiency (%)	40	48
Simulation average temperature on body (°C)	50.1	43.4

This study contributes to multiple sustainable development goals. The improvement of product efficiency reduces the cost and therefore helps Goal 7 which is affordable and clean energy and Goal 12 which is responsible consumption and production. In addition, a new design of components contributes to Goal 9 which is industry, innovation, and infrastructure. Furthermore, reducing the amount of copper used through effective cooling achieved by new fan design helps Goal 11 which is related to sustainability in cities and communities.

In conclusion, this study provided 8% fan efficiency, 18% volumetric flow rate, and 8 °C winding temperature improvement while keeping the motor efficiency the same. By reducing the winding temperature, approximately 1 kg of copper can be reduced from the coils in the motor core. Therefore, contribution to both sustainability targets and production efficiency are realized.

A future extension work on inclusion of the core geometry into the simulations can provide great benefits in detecting magnet temperatures in permanent magnet synchronous motors and can minimize the safety coefficients left in current designs.

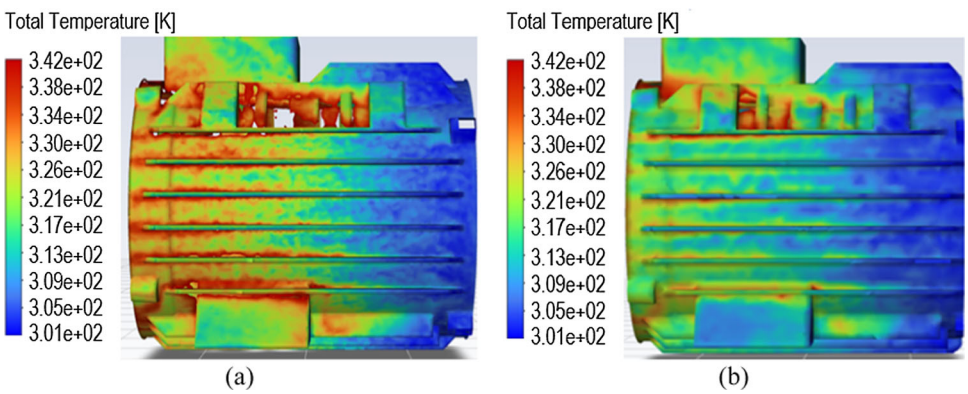

Fig. 13 The temperature distribution of the motor with **a** commercial fan and **b** optimized fan

Acknowledgements This study was carried out at WAT MOTOR Çerkezköy Factory.

Funding Open access funding provided by the Scientific and Technological Research Council of Türkiye (TÜBİTAK).

References

1. Bertoldi, P.; Trenev, G.: Preface. In Proceedings of the 8th International Conference EEMODS'2013 Energy Efficiency in Motor Driven Systems, pp. 1–8 (2014)
2. European Union, Commission Regulation (EU) 2019/1781. Official Journal of the European Union, pp. 1–21 (2019)
3. United Nations, "The 17 Goals", Department of Economic and Social Affairs Sustainable Development. https://sdgs.un.org/goals
4. Fan, Z.; Liu, G.; Jin, S.; Song, Z.; Wang, J.: Comparative study on torque characteristics of permanent magnet synchronous reluctance motors with different axial hybrid rotors. Energy Rep. **8**(5), 1349–1359 (2022). https://doi.org/10.1016/j.egyr.2022.03.023
5. Zhang, Y.; Wernicke, L.; Wulff, W.; Bleicher, A.; Schauer, T.: Design and validation of a dual-functional damper based on a stepper motor for energy harvesting and vibration control. Mech. Syst. Signal Process. **200**, 110568 (2023). https://doi.org/10.1016/j.ymssp.2023.110568
6. Attar, A.; Bouchnaif, J.; Grari, K.: Control of brushless DC motors using sensorless Back-EMF integration method. Mater. Today Proc. **8**, 7438–7443 (2021). https://doi.org/10.1016/j.matpr.2021.01.861
7. Rezaeealam, B.: Finite-element/boundary-element transient modelling of hysteresis motors. J. Magn. Magn. Mater. **519**, 167474 (2021). https://doi.org/10.1016/j.jmmm.2020.167474
8. Benedik, B.; Rihtaršič, J.; Povh, J.; Tavčar, J.: Failure modes and life prediction model for high-speed bearings in a through-flow universal motor. Eng. Fail. Anal. **128**, 105535 (2021). https://doi.org/10.1016/j.engfailanal.2021.105535
9. Monteagudo, F.E.L., et al.: Incidence of harmonic in asynchronous three-phase motors. Proc. Eng. **35**, 14–21 (2012). https://doi.org/10.1016/j.proeng.2012.04.160
10. Cabral, P.; Adouni, A.: Induction motor thermal analysis based on lumped parameter thermal network. In International Congress on Engineering- Engineering for Evolution, KnE Engineering, pp. 451–464 (2020) https://doi.org/10.18502/keg.v5i6.7061
11. Khiabani, A.; Alanis, D.A.: Cooling Fan Optimization for Heavy Electrified Vehicles: a study on performance and noise. Master's Thesis, School of Engineering Sciences Department of Aeronautical and Vehicle Engineering, KTH Royal Institute of Technology, Stockholm, Sweden (2020)
12. Anderson, K.; Lin, J.; McNamara, C.; Magri, V.: CFD study of forced air cooling and windage losses in a high speed electric motor. J. Elec. Cooling Therm. Control **5**, 27–44 (2015). https://doi.org/10.4236/jectc.2015.52003
13. Roffi, M.; Ferreira, F.J.T.E.; De Almeida, A.T.: "Comparison of different cooling fan designs for electric motors. In IEEE International Electric Machines and Drives Conference (IEMDC), Miami, FL, USA, pp. 1–7, (2017) https://doi.org/10.1109/IEMDC.2017.8002270
14. Jerzy, M.; Bartłomiej, B.: Air flow analysis for electrical motor's cooling system with autodesk simulation CFD 2013 program. Acta Mech. Auto. **7**, 89–92 (2013). https://doi.org/10.2478/ama-2013-0016
15. Hosain, M.L.; Fdhila, R.B.; Rönnberg, K.: Air-gap flow and thermal analysis of rotating machines using CFD. Energy Proc. **2017**(105), 5153–5159 (2017). https://doi.org/10.1016/j.egypro.2017.03.1045
16. Moon, S.H.; Jung, Y.H.; Kim, K.W.: Numerical investigation on thermal-flow characteristics of a totally enclosed fan cooled induction motor. In XXII International Conference on Electrical Machines (ICEM), Lausanne, Switzerland, pp. 1928–1933, (2016) https://doi.org/10.1109/ICELMACH.2016.7732787
17. Yoon, M.K.; Kauh, S.K.: Thermal analysis of a small totally enclosed fan cooled induction motor. Heat Transf. Eng. **26**, 77–86 (2006). https://doi.org/10.1080/01457630590916310
18. Ulbrich, S.; Kopte, J.; Proske, J.: Cooling fin optimization on a TEFC electrical machine housing using a 2-D conjugate heat transfer model. IEEE Trans. Ind. Electron. **65**(2), 1711–1718 (2018). https://doi.org/10.1109/TIE.2017.2748051
19. Galloni, E.; Parisi, P.; Marignetti, F.; Volpe, G.: CFD analyses of a radial fan for electric motor cooling. Therm. Sci. Eng. Prog. **8**, 470–476 (2018). https://doi.org/10.1016/j.tsep.2018.10.003
20. ANSYS, Ansys® Academic Research Mechanical, Release 2022 R2, (2022)
21. Nell, M.; Kubin, A.; Hameye, K.: Approach for the model and parameter selection for the calculation of induction machines. Energies **14**, 5623 (2021). https://doi.org/10.3390/en14185623
22. Cabral, P., AdouniInduction, A.: Motor thermal analysis based on lumped parameter thermal network", ICEUBI2019, In International Congress on Engineering—Engineering for Evolution Volume (2020)
23. Zumsteeg, M.; Karadzhi, S.: Technical Handbook Ventilation. Systemair (2019)
24. Morris, L.G.: The theory of fan ventilation. Acta Hortic. **22**, 74–85 (1971). https://doi.org/10.17660/ActaHortic.1971.22.12
25. Bergman, T.L.; Lavine, A.S.; Incropera, F.P.; DeWitt, D.P.: Fundamentals of Heat and Mass Transfer, 8th edn. Wiley, New Jersey (2018)
26. Fluent, A.F.: Theory guide. Release **R2**, 2021 (2021)
27. American Society of Heating, Refrigerating and Air-Conditioning Engineers, 2008 Ashrae Handbook: HVAC Systems and Equipment. Atlanta, GA, USA: ASHRAE, (2008)
28. Pascu, M.; Miclea, M.; Epple, P.; Delgado, A.; Durst, F.: Analytical and numerical investigation of the optimum pressure distribution along a low-pressure axial fan blade. Proc. Inst. Mech. Eng. C J. Mech. Eng. Sci. **223**, 643–657 (2009). https://doi.org/10.1243/09544062JMES1023
29. Belhocine, A.; Shinde, D.; Patil, R.: Thermo-mechanical coupled analysis based design of ventilated brake disc using genetic algorithm and particle swarm optimization. JMST Adv. **3**, 41–54 (2021). https://doi.org/10.1007/s42791-021-00040-0
30. Bagheri, M.; Jafari, A.A.; Sadeghifar, M.: A genetic algorithm optimization of ring-stiffened cylindrical shells for axial and radial buckling loads. Arch. Appl. Mech. **81**, 1639–1649 (2011). https://doi.org/10.1007/s00419-011-0507-2

31. Brighenti, R.; Carpinteri, A.; Vantadori, S.: A genetic algorithm applied to optimisation of patch repairs for cracked plates. Comput. Methods Appl. Mech. Eng. **196**, 466–475 (2006). https://doi.org/10.1016/j.cma.2006.07.004

32. Alperen, Y.; Sertac, C.: Multi objective optimization of a microchannel heat sink through genetic algorithm. Int. J. Heat Mass Transf. **146**, 118847 (2020). https://doi.org/10.1016/j.ijheatmasstransfer.2019.118847